Surface & Coatings Technology 356 (2018) 72–79

Contents lists available at ScienceDirect

Surface & Coatings Technology

journal homepage: www.elsevier.com/locate/surfcoat

Fabrication of calcite-coated rough-surface titanium using calcium nitrate

Rui Shi[a], Yuki Sugiura[a,b,*], Kanji Tsuru[a,c], Kunio Ishikawa[a]

[a] Department of Biomaterials, Faculty of Dental Science, Kyushu University, 3-1-1, Maidashi, Higashi-ku, Fukuoka 812-8534, Japan
[b] Health Research Institute, National Institute of Advance Industrial Science and Technology (AIST), 2217-14, Hayashi-cho, Takamatsu, Kagawa 761-0395, Japan
[c] Section of Bioengineering, Department of Dental Engineering, Fukuoka Dental College, 2-15-1, Tamura, Sawara-ku, Fukuoka 814-0193, Japan

ARTICLE INFO

Keywords:
Ti scaffold
Heat carbonation
Calcium carbonate
Coating
Surface structure
Calcite

ABSTRACT

Although Ti bone scaffolds are widely used clinically as various hard-tissue scaffolds including dental implants, their limited initial osseointegration property is a significant disadvantage, which should be improved. A rough surface and the allied Ca ion release capability might improve initial osteointegration by enhancing the activity of osteoblasts, which dominates osseointegration. In this study, a calcite-coating method, as a Ca ion releaser, is introduced onto rough surfaces of the Ti scaffold by heat carbonation using calcium nitrate as the Ca source below the α-to-β phase transition temperature (~880 °C) of Ti. After this treatment, the Ti scaffolds become whiter with increasing the concentration of the calcium nitrate solution. X-ray diffraction (XRD) and spectroscopic measurements demonstrate that calcite is formed on the Ti scaffold after the treatment. Scanning electron microscopy (SEM) observations show numerous rhombohedral crystals with a size of several micrometers, densely covering the surface of the Ti scaffold, maintaining its rough surface structure. Optimization of the initial calcium nitrate solution concentration controls the amount of calcite coating onto the desired regions on the surface of the Ti scaffolds. The coating strength of the fabricated calcite is ~20 MPa, which is sufficient to resist implanting strength.

1. Introduction

Ti and its alloys, such as Ti-6Al-4V, are widely used as hard-tissue scaffolds, such as bone scaffolds, surgical bolts, artificial joints, dental implants, and spinal gauges, because of their excellent biocompatibility and physico-chemical properties. Approximately, several tens of million people globally receive the benefit of the Ti scaffold every year [1–4].

Ti is used as a bone scaffold because it can directly connect to the bone tissue and attract it to the surrounding Ti regions when it is implanted into the bone, which is known as its osseointegration property [5–7]. However, the drawback of Ti is that its osseointegration property and its bone-contact ratio are limited; therefore, failure of the implanted tissues often occurs [8,9]. In particular, its low initial osseointegration property should be improved for future clinical use. [8,10–12].

Various studies have been performed to overcome the drawbacks of Ti and improve its biocompatibility. For example, when a rough textured surface is integrated on the Ti substrate, its osseointegration property is significantly increased [8,13–15]. In addition, the initial osseointegration property dominates the activity of cells acting in the bone-remodeling process. Their activities are closely related to the Ca concentration in the surrounding microenvironment of scaffolds [16–18]. In fact, Chen et al. [19] suggested that Ca ions released from implanted materials can enhance the activity of cells dominating the bone-remodeling process by stimulating their bone matrix protein 2 (BMP2) signaling pathway. Moreover, Hong et al. [20] reported that when a suitable amount of Ca is released from the alloy, it enhances the activity of rat osteoblastic cell-obtained rat calvaria bone marrow (MC3T3-E1 cell) in vitro.

Calcite is a polymorph of calcium carbonate found as a robust crystal with relatively high solubility under physiological conditions [21–23]. In addition, calcite itself has been already used as a bone substitute, revealing excellent initial osteoconductivity and bone-replacing rate [24–26]. Liu et al. [27] demonstrated a calcium carbonate-coated Ti plate, using a calcium carbonate precipitation method on a Ti plate immersed in a $CaCl_2$ aqueous solution by exposing it to a $(NH_4)_2CO_3$ stream. Although the calcium carbonate coating using the precipitation method enhanced the activity of osteoblastic cells, the coating shape and the amount of calcium carbonate were not very well regulated.

Therefore, in this study, we focus on establishing a method for generating uniform calcite coatings with Ca amount regulation using a

* Corresponding author at: Health Research Institute, National Institute of Advance Industrial Science and Technology (AIST), 2217-14, Hayashi-cho, Takamatsu, Kagawa 761-0395, Japan.
E-mail address: yuki-sugiura@aist.go.jp (Y. Sugiura).

https://doi.org/10.1016/j.surfcoat.2018.09.050
Received 11 July 2018; Received in revised form 20 September 2018; Accepted 21 September 2018
Available online 22 September 2018

calcium nitrate solution as a starting material. Treated Ti substrates with rough-textured surfaces were coated with calcite, maintaining the underlying roughness through a thermal carbonation process.

2. Material and methods

2.1. Materials

Commercial pure Ti (bare Ti) plates (T&I Co., Japan) squares with an area of 100 mm^2 were used as the coating substrates. $Ca(NO_3)_2{\cdot}4H_2O$ (Wako Pure Inc., Co., Japan) was dissolved in 99.5% ethanol (EtOH) to obtain 0.5, 1.0, and 2.0 mol/L $Ca(NO_3)_2{\cdot}4H_2O$-EtOH solution as the Ca source.

2.2. Acid etching of bare Ti

A bare Ti plate was immersed in a cocktail acid solution of 50 v% H_2SO_4 and 7 v% HCl at 70 °C for 30 min to obtain etched texture on its surface. After acid etching, the etched Ti plate (Etched Ti) was washed in ethanol (70%) with ultrasonic treatment for 5 min and then washed in distilled water with ultrasonic treatment for 5 min. After washing, Etched Ti was placed at room temperature for drying.

2.3. Heating treatment for carbonation

For this, 5 μL of 0.5–2.0 mol/L $Ca(NO_3)_2{\cdot}4H_2O$-EtOH solutions were dropped onto the center of Etched Ti, following which the solvent was evaporated at room temperature to obtain the $Ca(NO_3)_2{\cdot}4H_2O$ precipitate on the Etched Ti surface.

After the treatment by the $Ca(NO_3)_2{\cdot}4H_2O$-EtOH solutions, Etched Ti and a control sample of Etched Ti without treatment were placed into an electric furnace (Mini-1, Nitto Kagaku Co., Japan) with a modified step controller (NPC-T03, Nitto Kagaku Co., Japan). The temperature of the furnace was increased from the room temperature to 550 °C at 3 °C/min and then maintained at 550 °C for 5 h with a CO_2 gas flow of 100 mL/min. Subsequently, the samples were cooled down inside the furnace.

2.4. Characterization

The surface materials obtained by the treatments were characterized by X-ray diffraction (XRD; D08 ADVANCE, Bruker AXS GmbH, Germany) at an acceleration voltage of 40 kV and a current of 40 mA using a Cu target. The 2θ range measurement was from 10° to 70° with an increment of 0.02°; the time per step was 3°/min. The samples were placed onto the XRD stage without any further treatment.

The surface morphology of the samples was observed by scanning electron microscopy (SEM; S-3400 N, Hitachi Hightech Co., Japan) at an acceleration voltage of 15 kV after Au/Pd sputter coating by a magnetron sputtering device (MSP-1, Vacuum Device Co., Japan). The elemental mapping of the samples was performed using energy-dispersed X-ray spectroscopy (EDX; EDAX GENESIS4000, EDAX Japan Co., Japan) combined with SEM at an acceleration voltage of 15 kV. The surface elemental analysis was performed and the coating structure was obtained using an X-ray photoelectron spectrometer (XPS: K-Alpha, ThermoFisher Scientific Co., USA) equipped with a monochromatic X-ray source (Al-Kα) at 12 kV, 6 mA under a pressure of 1.4×10^{-6} Pa. The spot size of the incident beam was set to 400 μm. The binding energies were normalized to the C1s peak of 284.80 eV. The surface chemical bonding structure of the samples was determined by laser Raman spectroscopy (Raman: NRS-3100CS, Jasco Co., Japan) using a GaAs laser (wavelength: 784 nm) and a charge coupled device (CCD) detector (two accumulate scans, resolution: 0.02 cm^{-1}). In the XPS and Raman measurements, reference $CaCO_3$ was used, a calcite single crystal obtained from *Saidosho-Mine, Kaharu-cho, Fukuoka, Japan*.

For material reaction estimation during the heat treatment, the samples were measured using thermogravimetric analysis (TG-DTA; EXSTAR TG/DTA6300, SII Nano Technology Inc., Japan) under a stream of air or CO_2. The heating rate was the same as that of the sample fabrication.

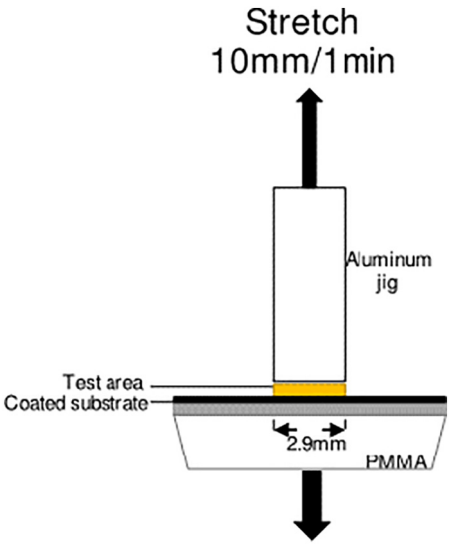

Scheme 1. Schematic image of the detaching test.

The surface roughness R_a of the samples was measured by surface roughness-measuring machines (SJ-400, Mitutoyo Co., Japan). An average value of R_a was calculated from a line on each sample ($n = 5$).

An adhesion test apparatus was used to measure the adhesive bonding strength of the coating and the Ti substrate. The scheme of the measurement is shown in Scheme 1. A commercial cylindrical aluminum rod of 2.9 mm in diameter was attached to the surface of the sample by a thin layer of epoxy resin (Araldite AR-1600, Hantzman Co., Switzerland). The rate of stretching was controlled at 10 mm/min by a universal testing machine (AGS-J, Shimadzu Co., Japan). The maximum load was recorded until the rod detached from the surface of the sample ($n = 4$). After the measurement, the surfaces of the samples were observed by SEM.

3. Results

Fig. 1. summarizes the TG-DTA curves of the thermal gradient and time evolution at ~550 °C of Etched Ti without $Ca(NO_3)_2{\cdot}4H_2O$ in an air stream (a, b) and in a CO_2 flow (c, d) as well as with $Ca(NO_3)_2{\cdot}4H_2O$ in an air stream (e, f) and in a CO_2 flow (g, h). In the case of Ti without Ca $(NO_3)_2{\cdot}4H_2O$, either in air or CO_2, neither a slight weight change nor thermal differentiation was observed. Whereas, in the case of Ti with Ca $(NO_3)_2{\cdot}4H_2O$, either in air or CO_2, three significant weight loss steps at around 80–120, 120–150, and 500–550 °C, corresponding to moisture evaporation, crystal water evaporation, and $Ca(NO_3)_2$ decomposition, respectively, were observed. The TG-DTA analysis also indicated that at least 1 h is required for complete decomposition of $Ca(NO_3)_2$ at ~550 °C.

Fig. 2. shows the photographs of bare Ti (a) and Etched Ti before the heat treatment (b), Etched Ti after the heat treatment without Ca $(NO_3)_2{\cdot}4H_2O$ (c), with 0.5 mol/L $Ca(NO_3)_2{\cdot}4H_2O$ (d), with 1.0 mol/L Ca $(NO_3)_2{\cdot}4H_2O$ (e), and with 2.0 mol/L $Ca(NO_3)_2{\cdot}4H_2O$ (f). Bare Ti has a greyish smooth surface with bright metallic luster, whereas Etched Ti shows a dark brown-colored surface without any metallic luster. Although the surface color was essentially the same after carbonation without $Ca(NO_3)_2{\cdot}4H_2O$ solution treatment, the color of the Etched Ti samples after carbonation with the 0.5 mol/L $Ca(NO_3)_2{\cdot}4H_2O$ solution treatment was revealed to be uniformly whitish. Furthermore, in addition to this tendency, a scaly texture which pseudomorphic remain of

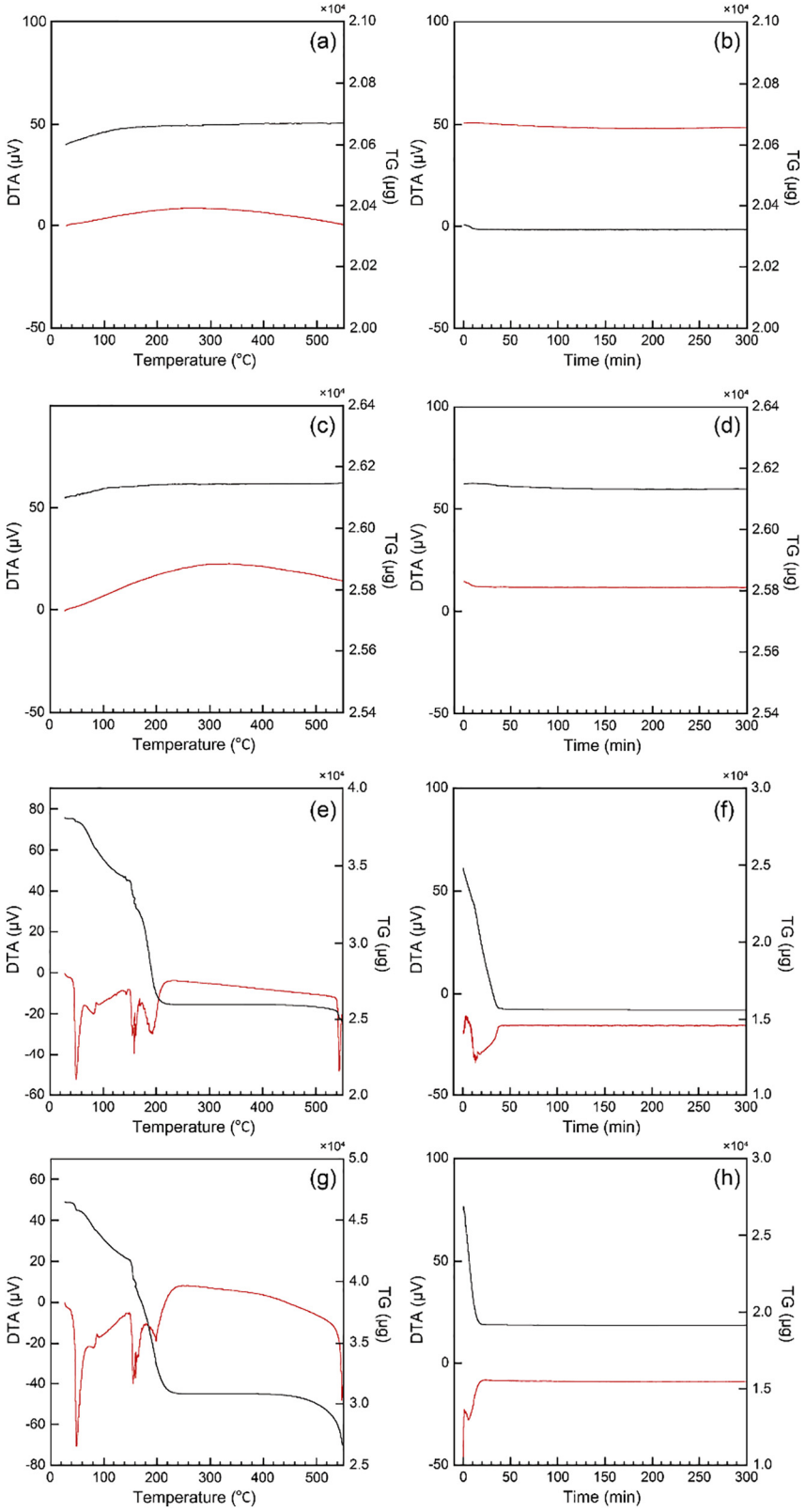

Fig. 1. TG-DTA curves of the thermal gradient and time evolution at ~550 °C for Etched Ti without $Ca(NO_3)_2{\cdot}4H_2O$ in an air stream (a, b) and in a CO_2 flow (c, d) as well as with $Ca(NO_3)_2{\cdot}4H_2O$ in an air stream (e, f) and in a CO_2 flow (g, h). Black line: TG curve, red line: DTA curve. (For interpretation of the references to color in this figure legend, the reader is referred to the web version of this article.)

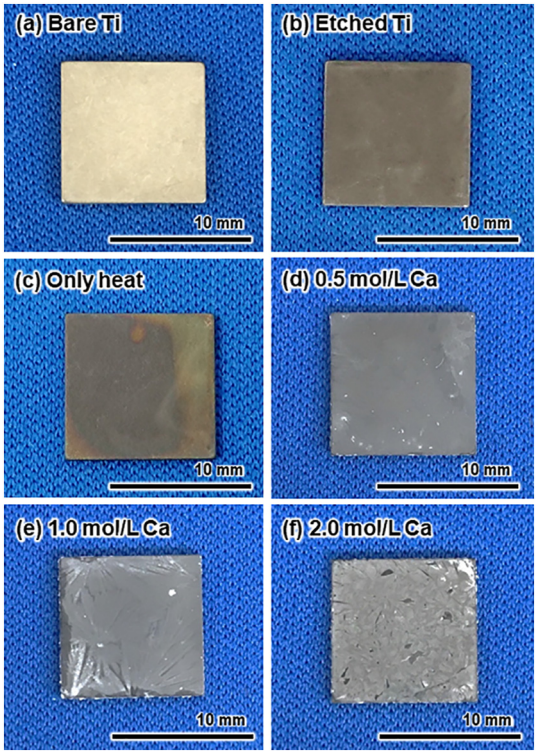

Fig. 2. Photographs of bare Ti (a), Etched Ti (b), Etched Ti with heating, without a $Ca(NO_3)_2{\cdot}4H_2O$ solution (c), with 0.5 mol/L $Ca(NO_3)_2{\cdot}4H_2O$ solution (d), 1.0 mol/L $Ca(NO_3)_2{\cdot}4H_2O$ solution (e), and 2.0 mol/L $Ca(NO_3)_2{\cdot}4H_2O$ (f).

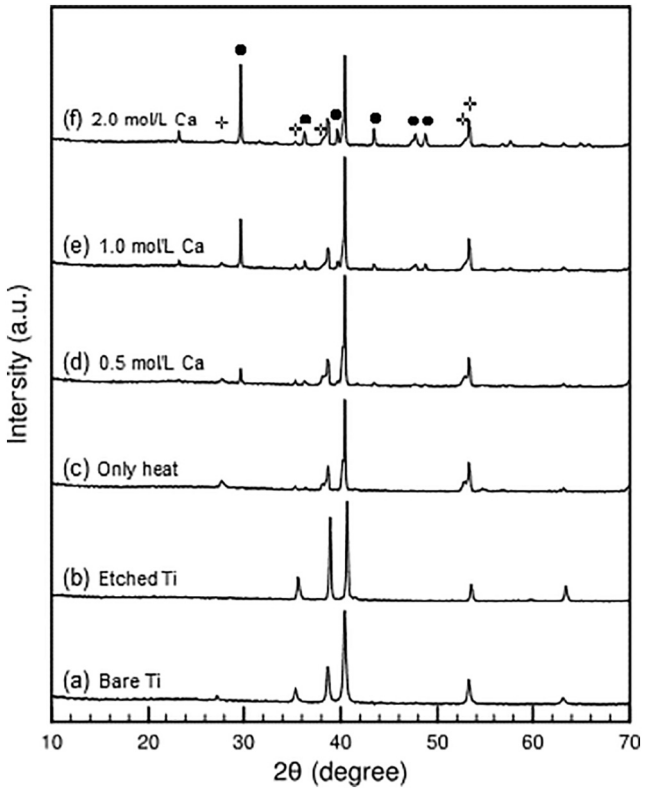

Fig. 3. Normal XRD pattern of bare Ti (a), Etched Ti (b), Etched Ti with heating, without a $Ca(NO_3)_2{\cdot}4H_2O$ solution (c), with 0.5 mol/L $Ca(NO_3)_2{\cdot}4H_2O$ solution (d), with 1.0 mol/L $Ca(NO_3)_2{\cdot}4H_2O$ solution (e), and with 2.0 mol/L Ca $(NO_3)_2{\cdot}4H_2O$ (f). ●: calcite, ✣: TiO_2 (rutile and anatase).

$Ca(NO_3)_2{\cdot}4H_2O$ appeared on Etched Ti after heating with the increase in the concentration of the $Ca(NO_3)_2{\cdot}4H_2O$ solution in the preceding treatment.

Fig. 3. shows the XRD patterns of bare Ti (a) and Etched Ti before the heat treatment (b), after the heat treatment without $Ca(NO_3)_2{\cdot}4H_2O$ (c), with 0.5 mol/L $Ca(NO_3)_2{\cdot}4H_2O$ (d), with 1.0 mol/L $Ca(NO_3)_2{\cdot}4H_2O$ (e), and with 2.0 mol/L $Ca(NO_3)_2{\cdot}4H_2O$ (f). The etched Ti samples generated via heating with $Ca(NO_3)_2{\cdot}4H_2O$ showed calcite and Ti peaks. The intensity of the calcite peaks increased with increasing the concentration of the $Ca(NO_3)_2{\cdot}4H_2O$-EtOH treatment solutions. In addition, after the heating, the peaks of TiO_2 phases (i.e., rutile and anatase) appeared.

Fig. 4. shows the XPS spectra of wide range (a), Ti2p (b) and Ca2p (c), of the samples and single calcite crystal as a reference. The wide range XPS spectra of the samples indicate a significant difference between the samples without Ca treatment and without Ca treatment. In the case of bare Ti, Etched Ti, and only heated Ti, they clearly show Ti peaks, but no Ca peaks. On the other hand, in the case of Ca-treated Ti, they show no Ti peaks, but clear Ca peaks. This phenomenon indicated that the Ti plate surface was completely coated by Ca-containing materials.

Fig. 5 shows the Raman spectra of bare Ti (a) and Etched Ti before the heat treatment (b), after the heat treatment without $Ca(NO_3)_2{\cdot}4H_2O$ (c), with 0.5 mol/L $Ca(NO_3)_2{\cdot}4H_2O$ (d), with 1.0 mol/L $Ca(NO_3)_2{\cdot}4H_2O$ (e), and with 2.0 mol/L $Ca(NO_3)_2{\cdot}4H_2O$ (f), and single calcite crystal as a reference (g). The same as the XPS result, bare Ti, Etched Ti, and only heated Ti show no calcite peaks, whereas the Ca-treated samples show clear calcite peaks at 720 cm^{-1} and 1085 cm^{-1}. The intensities of the calcite peaks of the samples are increased with the treated Ca $(NO_3)_2{\cdot}4H_2O$ concentrations.

Fig. 6 shows the SEM micrographs of bare Ti (a, b) and Etched Ti before the heat treatment (c, d), after the heat treatment without Ca $(NO_3)_2{\cdot}4H_2O$ (e, f), with 0.5 mol/L $Ca(NO_3)_2{\cdot}4H_2O$ (g, h), with 1.0 mol/L $Ca(NO_3)_2{\cdot}4H_2O$ (i, j), and with 2.0 mol/L $Ca(NO_3)_2{\cdot}4H_2O$ (k, l). Etched Ti has block-like textures ranging from ~10 μm to Ti crystal grains with numerous nanometer-sized rough structures, whereas bare Ti has a smooth surface. The block-like texture observed on the surface of Etched Ti was clearly maintained during the heat treatment without $Ca(NO_3)_2{\cdot}4H_2O$ pre-treatment. The samples treated with 0.5 and 1.0 mol/L $Ca(NO_3)_2{\cdot}4H_2O$ were coated with rhombohedral crystals ~1 μm on the surfaces of the samples, while maintaining the block-like texture of Etched Ti. However, the sample of 2.0 mol/L $Ca(NO_3)_2{\cdot}4H_2O$ was uniformly covered with rhombohedral crystals, as shown for the low-concentration samples. The block-like texture of Etched Ti in the sample of 2.0 mol/L $Ca(NO_3)_2{\cdot}4H_2O$ was barely observable. In addition, an extra layer consisting of rhombohedral crystals on the surface was observed.

Fig. 7. shows the surface roughness values R_a of the samples. The R_a values of bare Ti and Etched Ti are 0.46 ± 0.02 μm and 1.75 ± 0.32 μm, respectively. In other words, after acid etching, the R_a value of the samples significantly increased. Whereas, the R_a values of Etched Ti after the heat treatment without $Ca(NO_3)_2{\cdot}4H_2O$, with 0.5 mol/L, and 1.0 mol/L $Ca(NO_3)_2{\cdot}4H_2O$ are 1.63 ± 0.12, 1.78 ± 0.26, and 1.83 ± 0.18 μm, respectively. These R_a values were not significantly different compared to those of Etched Ti. The R_a value of Etched Ti after the heat treatment with 2.0 mol/L $Ca(NO_3)_2{\cdot}4H_2O$ was 2.60 ± 0.12 μm, which is significantly higher than those of the low-concentration $Ca(NO_3)_2{\cdot}4H_2O$ treatments.

Fig. 8. shows the cross-sectional SEM micrograph and the elemental mapping by EDX analysis of Etched Ti after the heat treatment with 0.5 mol/L $Ca(NO_3)_2{\cdot}4H_2O$. The thickness of the coating layer is < 5 μm. The elemental mapping analysis clearly indicates that the coating layer contains Ca, C, and O on the Ti surface. The cross-sectional micrograph also reveals that there is no gap between the coating layer and the Ti substrate.

Fig. 9. shows the adhesive strength between the coating and

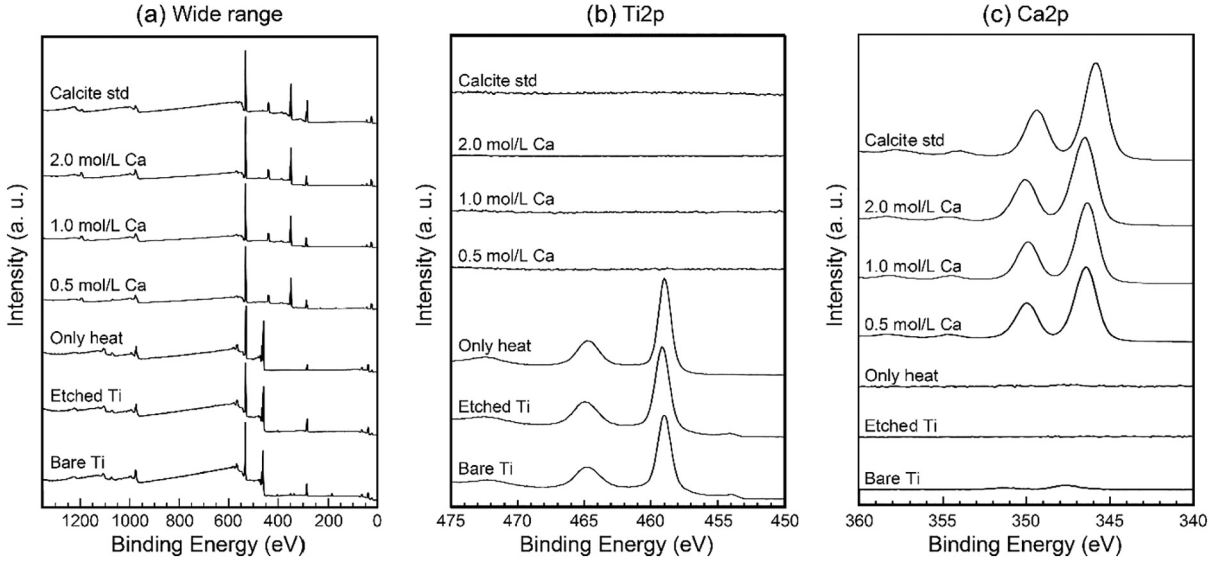

Fig. 4. XPS spectra of the samples and calcite std. for facilitate comparison. (a) Full wide. (b) Ti2p. (c) Ca2p.

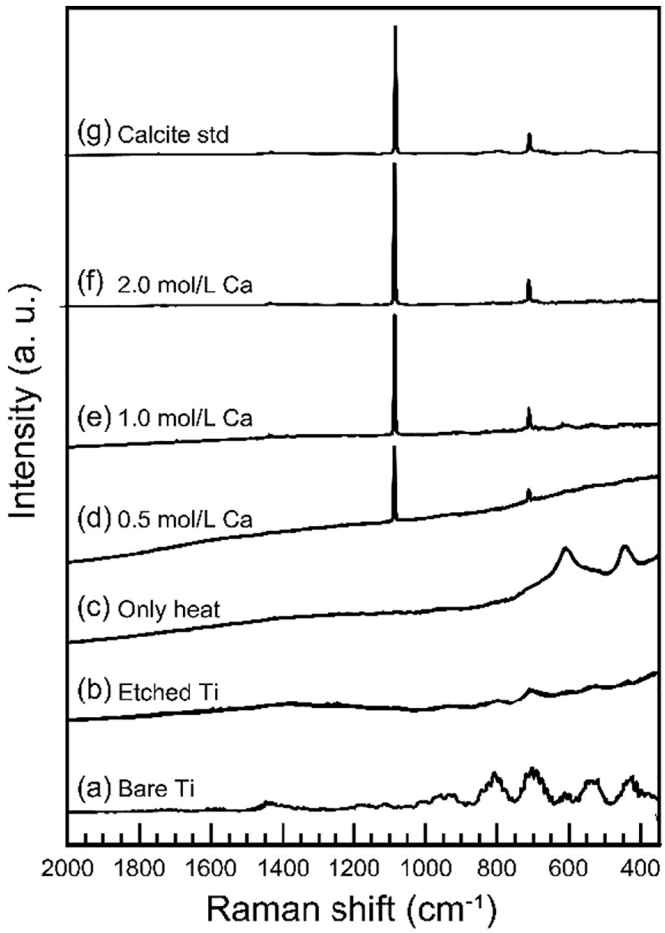

Fig. 5. Raman spectra of bare Ti (a), Etched Ti (b), Etched Ti with heating, without a $Ca(NO_3)_2{\cdot}4H_2O$ solution (c), with 0.5 mol/L $Ca(NO_3)_2{\cdot}4H_2O$ solution (d), with 1.0 mol/L $Ca(NO_3)_2{\cdot}4H_2O$ solution (e), with 2.0 mol/L $Ca(NO_3)_2{\cdot}4H_2O$ (f), and calcite std. (g) for facilitate comparison.

substrate of Etched Ti treated with 0.5 mol/L, 1.0 mol/L, and 2.0 mol/L $Ca(NO_3)_2{\cdot}4H_2O$; the adhesive strengths of these treated samples are 21.90 ± 2.11, 10.46 ± 1.60, and 5.84 ± 0.52 MPa, respectively. To confirm the test mode of the adhesive strength, Etched Ti was used as a control sample. Its adhesive strength is 18.10 ± 1.39 MPa. To determine the fracture modes of each sample, we observed the surface of the samples after adhesive testing.

Fig. 10. shows the SEM micrographs of not treated Etched Ti and Etched Ti treated with different concentrations of $Ca(NO_3)_2{\cdot}4H_2O$ after the adhesive testing. In the cases of Etched Ti and Etched Ti treated with 0.5 mol/L $Ca(NO_3)_2{\cdot}4H_2O$, some broken areas of the binder are clearly observed. In the samples treated with 1.0 or 2.0 mol/L Ca $(NO_3)_2{\cdot}4H_2O$, few remaining binder, fractured coating layer, and lower Ti substrate are observed, whereas almost only the fractured coating layer is observed for the sample treated with 2.0 mol/L $Ca(NO_3)_2{\cdot}4H_2O$. These results indicate that the crystals were still firmly attached to the surface of Ti even though we observe that the crystals themselves were broken. The fracture modes of each sample are summarized in Table 1.

4. Discussion

The obtained results clearly indicate that calcite can be tightly and uniformly coated onto a Ti substrate, maintaining its surface structure, using our method. The surface structure of the Ti substrate plays an essential role in osseointegration. [14,28] The basic concept of this coating technique is the induction of thermal decomposition of Ca $(NO_3)_2{\cdot}4H_2O$ in a CO_2 gas environment. It is known that when Ca $(NO_3)_2{\cdot}4H_2O$ is heated above ~500 °C [29], it decomposes to CaO, as shown in Eq. (1):

$$2Ca(NO_3)_2{\cdot}4H_2O \rightarrow 2CaO + 4\,NO_2 + O_2 + 8H_2O \quad (1)$$

Resulting CaO can react with surrounding CO_2, so that $CaCO_3$ is deposited on the Ti substrate, as shown in Eq. (2):

$$CaO + CO_2 \rightarrow CaCO_3 \quad (2)$$

This enables the induction of the carbonation reaction below the α–β Ti transition temperature (~880 °C) causing degradation of the Ti mechanical strength [30]. Furthermore, several studies indicated that residual TiO_2 could improve the osteoconductivity of scaffolds [31,32].

The TG-DTA results show that in the case of the CO_2 flow system, there is no significant weight increase corresponding to carbonation of CaO. Therefore, these reactions occur at relatively low temperatures (~200 °C). In other words, direct carbonation from calcium nitride, probably in an anhydride phase, could enable the formation of calcite on the Ti surface. In addition, the TG-DTA results indicate that CaO formed via decomposition of calcium nitride also reacted with CO_2 simultaneously, becoming calcite.

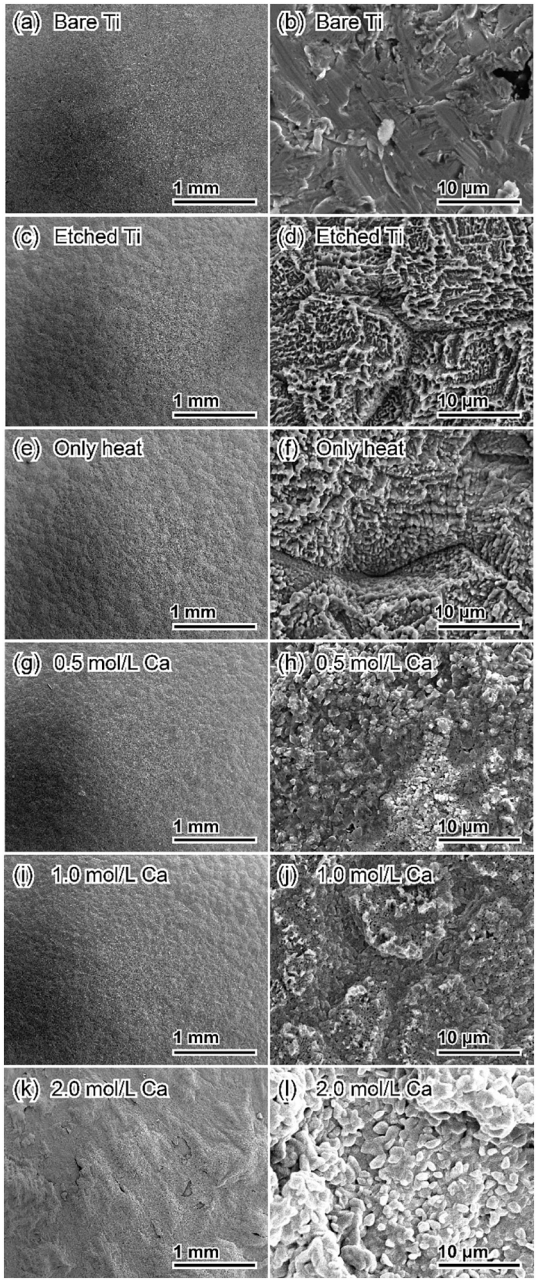

Fig. 6. SEM micrograph of bare Ti (a, b), Etched Ti (c, d), Etched Ti with heating, without a $Ca(NO_3)_2{\cdot}4H_2O$ solution (e, f), with 0.5 mol/L $Ca(NO_3)_2{\cdot}4H_2O$ solution (g, h), with 1.0 mol/L $Ca(NO_3)_2{\cdot}4H_2O$ solution (i, j), and with 2.0 mol/L $Ca(NO_3)_2{\cdot}4H_2O$ (k, l).

Therefore, calcite can be coated onto Ti by the heat treatment using a $Ca(NO_3)_2{\cdot}4H_2O$ solution. Based only on the material science aspect, above 2.0 mol/L $Ca(NO_3)_2{\cdot}4H_2O$ as a Ca source, the coating is too thick and weak because of sedimentary accumulation structure. Therefore, it seems that the application of below 2.0 mol/L $Ca(NO_3)_2{\cdot}4H_2O$ is the optimal way for this coating. When it is used for a hard-tissue scaffold through implantation, it is absolutely needed to perform in vitro/in vivo evaluation for optimizing the coating amount. Our further study will show the optimal Ca concentration for calcite coating on the Ti substrate. In this study, we established the simple calcite-coating method of controlling the concentration or amount of the Ca $(NO_3)_2{\cdot}4H_2O$ solution for immersion, which enables optimization not only of the calcite-coating amount, but also of the surface structure of the Ti substrate, which enhances its biocompatibility.

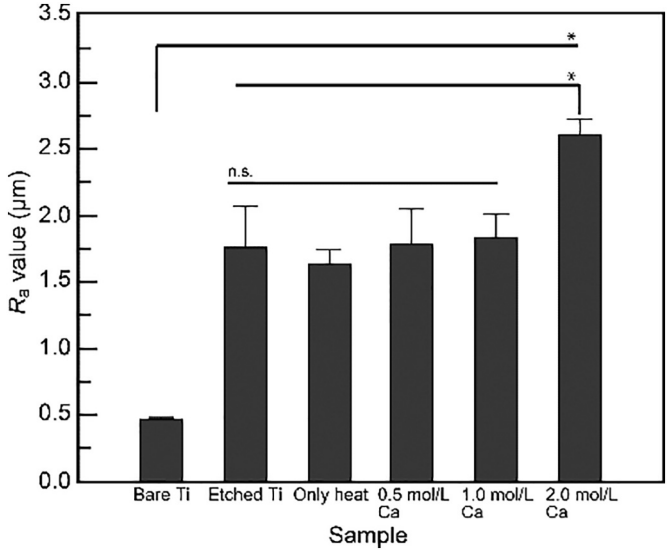

Fig. 7. Surface roughness R_a of bare Ti plate, Etched Ti, Etched Ti with heating, without a $Ca(NO_3)_2{\cdot}4H_2O$ solution, with 0.5 mol/L $Ca(NO_3)_2{\cdot}4H_2O$ solution, 1.0 mol/L $Ca(NO_3)_2{\cdot}4H_2O$ solution, and with 2.0 mol/L $Ca(NO_3)_2{\cdot}4H_2O$. *Statistically significant difference between the connected value ($p < 0.05$, $n = 5$).

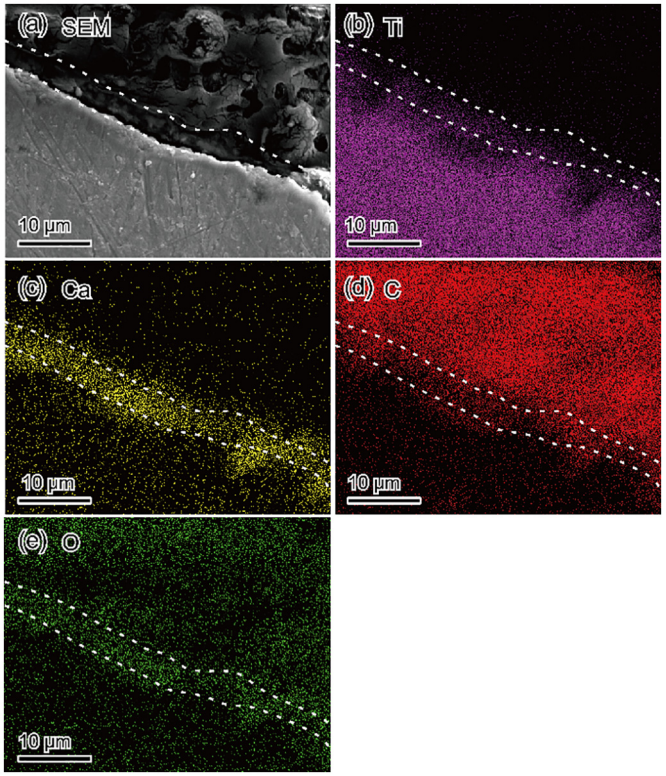

Fig. 8. Cross-sectional SEM (a); its EDX mapping of Ti (b), Ca (c), C (d), and O (e) of Etched Ti with heating with 0.5 mol/L $Ca(NO_3)_2{\cdot}4H_2O$ solution.

The coating strength of the fabricated $CaCO_3$ coating on the Ti substrate maintaining its surface structure is ~20.0 MPa. This coating strength is not inferior to the coating strengths of other ceramics coating, such as hydroxyapatite (HAp; ~9 MPa) on Ti fabricated by a plasma-spray method and $ZnPO_4$ on stainless steel manufactured via hydrothermal treatment (~12.0 MPa), which are already commercialized or categorized as eternal coatings [33,34]. Therefore, a $CaCO_3$ coating on a Ti substrate fabricated using our technique has a sufficient

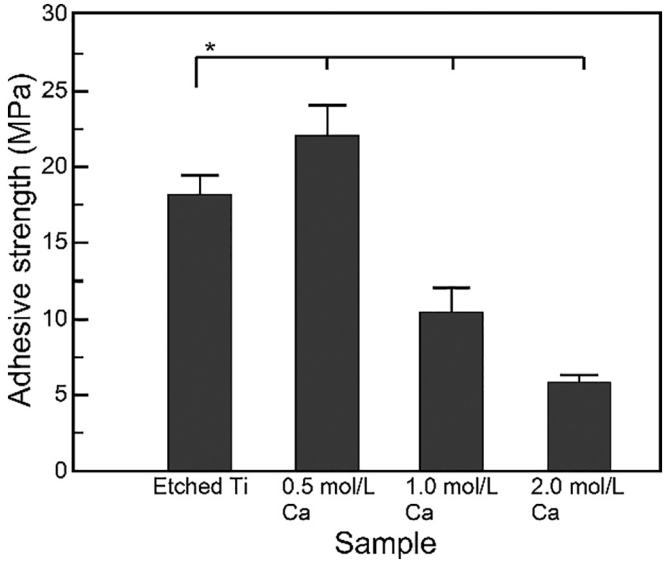

Fig. 9. Adhesive strength of Etched Ti after heating with 0.5, 1.0, 2.0 mol/L Ca $(NO_3)_2{\cdot}4H_2O$ ($p > 0.05$, $n = 4$).

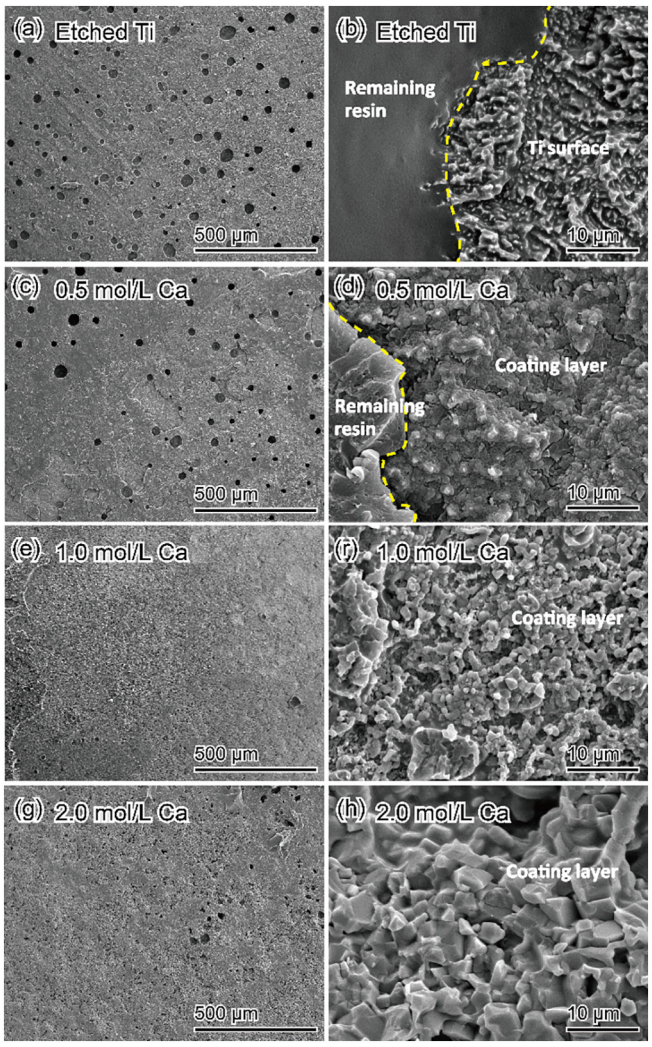

Fig. 10. SEM micrographs of the surface after the adhesive test: Etched Ti (a, b), Etched Ti with 0.5 mol/L $Ca(NO_3)_2{\cdot}4H_2O$ solution (c, d), Etched Ti with 1.0 mol/L $Ca(NO_3)_2{\cdot}4H_2O$ solution (e, f), and Etched Ti with 2.0 mol/L Ca $(NO_3)_2{\cdot}4H_2O$ solution (g, h).

Table 1
Summary of the fracture modes for each sample.

Sample	Fracture mode
Etched Ti	Between Al jig and resin
0.5 mol/L Ca	Between Al jig and resin
1.0 mol/L Ca	Inside of calcite coating
2.0 mol/L Ca	Inside of calcite coating

strength for implantation.

5. Conclusion

In conclusion, a $CaCO_3$ coating layer was successfully prepared on a Ti substrate by heat treatment at 550 °C for 3 h in the presence of CO_2 gas flow of 100 mL/min using a $Ca(NO_3)_2{\cdot}4H_2O$ ethanolic solution as a Ca source. The adhesive test indicates that the coating layer has a sufficient coating strength on the Ti substrate for implantation. By optimizing the concentration of the ethanolic $Ca(NO_3)_2{\cdot}4H_2O$ solution, the calcite coating could be fabricated on the Ti substrate maintaining the surface block texture of the underlying substrate that may play an essential role in osseointegration.

Acknowledgement

This research was supported by Japan Agency for Medical Research and Development (AMED), Japan under Grant Number JP18im0502004 for K.I., by a Grant-in-Aid for KAKENHI, Young Researcher (B) (JP16K20505), Japan Society for the Promotion of Science (JSPS) for Y.S. and, China Scholarships Council (CSC, No.201708050163) by Chinese Ministry of Education for R.S.

References

[1] M. Geetha, A.K. Singh, R. Asokamani, A.K. Gogia, Ti based biomaterials, the ultimate choice for orthopaedic implants — a review, Prog. Mater. Sci. 54 (2009) 397–425.
[2] M. Semlitsch, Titanium alloys for hip joint replacements, Clin. Mater. 2 (1987) 1–13.
[3] J. Witt, M. Swann, Metal wear and tissue response in failed titanium alloy total hip replacements, Bone & Joint Journal 73 (1991) 559–563.
[4] H. Nakajima, T. Okabe, Titanium in dentistry, Dent. Mater. J. 15 (1996) 77.
[5] R.Z. LeGeros, R.G. Craig, Strategies to affect bone remodeling: osteointegration, J. Bone Miner. Res. 8 (1993).
[6] R.K. Schenk, D. Buser, Osseointegration: a reality, Periodontology 2000 (17) (1998) 22–35.
[7] L. Carlsson, T. Röstlund, B. Albrektsson, T. Albrektsson, P.-I. Brånemark, Osseointegration of titanium implants, Acta Orthop. Scand. 57 (1986) 285–289.
[8] T. Albrektsson, P.-I. Brånemark, H.-A. Hansson, J. Lindström, Osseointegrated titanium implants: requirements for ensuring a long-lasting, direct bone-to-implant anchorage in man, Acta Orthop. Scand. 52 (1981) 155–170.
[9] N.P. Lang, G.E. Salvi, G. Huynh-Ba, S. Ivanovski, N. Donos, D.D. Bosshardt, Early osseointegration to hydrophilic and hydrophobic implant surfaces in humans, Clin. Oral Implants Res. 22 (2011) 349–356.
[10] P.R. Klokkevold, R.D. Nishimura, M. Adachi, A. Caputo, Osseointegration enhanced by chemical etching of the titanium surface. A torque removal study in the rabbit, Clin. Oral Implants Res. 8 (1997) 442–447.
[11] T. Jinno, V.M. Goldberg, D. Davy, S. Stevenson, Osseointegration of surface-blasted implants made of titanium alloy and cobalt–chromium alloy in a rabbit intramedullary model, J. Biomed. Mater. Res. A 42 (1998) 20–29.
[12] L.L. Guehennec, A. Soueidan, P. Layrolle, Y. Amouriq, Surface treatments of titanium dental implants for rapid osseointegration, Dent. Mater. 23 (2007).
[13] A.L. Rosa, M.M. Beloti, Rat bone marrow cell response to titanium and titanium alloy with different surface roughness, Clin. Oral Implants Res. 14 (2003) 43–48.
[14] C. Wirth, B. Grosgogeat, C. Lagneau, N. Jaffrezic-Renault, L. Ponsonnet, Biomaterial surface properties modulate in vitro rat calvaria osteoblasts response: roughness and or chemistry? Mater. Sci. Eng. C 28 (2008) 990–1001.
[15] D. Buser, R. Schenk, S. Steinemann, J. Fiorellini, C. Fox, H. Stich, Influence of surface characteristics on bone integration of titanium implants. A histomorphometric study in miniature pigs, J. Biomed. Mater. Res. A 25 (1991) 889–902.
[16] K. Ishikawa, N. Koga, K. Tsuru, I. Takahashi, Fabrication of interconnected porous calcite by bridging calcite granules with dicalcium phosphate dihydrate and their histological evaluation, J. Biomed. Mater. Res. A 104 (2016) 652–658.
[17] R.Z. LeGeros, Calcium phosphate-based osteoinductive materials, Chem. Rev. 108 (2008) 4742–4753.

[18] P. Ducheyne, Q. Qiu, Bioactive ceramics: the effect of surface reactivity on bone formation and bone cell function, Biomaterials 20 (1999) 2287–2303.
[19] Z. Chen, C. Wu, W. Gu, T. Klein, R. Crawford, Y. Xiao, Osteogenic differentiation of bone marrow MSCs by β-tricalcium phosphate stimulating macrophages via BMP2 signalling pathway, Biomaterials 35 (2014) 1507–1518.
[20] D. Hong, D.-T. Chou, O.I. Velikokhatnyi, A. Roy, B. Lee, I. Swink, I. Issaev, H.A. Kuhn, P.N. Kumta, Binder-jetting 3D printing and alloy development of new biodegradable Fe-Mn-Ca/Mg alloys, Acta Biomater. 45 (2016) 375–386.
[21] R. Narayanan, S. Seshadri, T. Kwon, K. Kim, Calcium phosphate-based coatings on titanium and its alloys, J Biomed Mater Res B Appl Biomater 85 (2008) 279–299.
[22] R. Chang, S. Kim, S. Lee, S. Choi, M. Kim, Y. Park, Calcium carbonate precipitation for CO_2 storage and utilization: a review of the carbonate crystallization and polymorphism, Frontiers in Energy Research 17 (2017), https://doi.org/10.3389/fenrg.2017.00017.
[23] R.A. Yukna, Clinical evaluation of coralline calcium carbonate as a bone replacement graft material in human periodontal osseous defects, J. Periodontol. 65 (1994) 177–185.
[24] K. Ishikawa, N.X.T. Tram, K. Tsuru, R. Toita, Fabrication of porous calcite using chopped nylon fiber and its evaluation using rats, J. Mater. Sci. Mater. Med. 26 (2015) 94.
[25] G. Guillemin, J.L. Patat, J. Fournie, M. Chetail, The use of coral as a bone graft substitute, J. Biomed. Mater. Res. A 21 (1987) 557–567.
[26] Y. Fujita, T. Yamamuro, T. Nakamura, S. Kotani, C. Ohtsuki, T. Kokubo, The bonding behavior of calcite to bone, J. Biomed. Mater. Res. 25 (1991) 991–1003.
[27] Y. Liu, T. Jiang, Y. Zhou, Z. Zhang, Z. Wang, H. Tong, X. Shen, Y. Wang, Evaluation of the attachment, proliferation, and differentiation of osteoblast on a calcium carbonate coating on titanium surface, Mater. Sci. Eng. C 31 (2011) 1055–1061.
[28] A. Wennerberg, T. Albrektsson, Effects of titanium surface topography on bone integration: a systematic review, Clin. Oral Implants Res. 20 (Suppl. 4) (2009) 172–184.
[29] K.H. Stern, High temperature properties and decomposition of inorganic salts part 3, nitrates and nitrites, J. Phys. Chem. Ref. Data 1 (1972) 756–757.
[30] A. Prince, G.V. Raynor, D.S. Evans, I.o. Metals, Phase Diagrams of Ternary Gold Alloys, Institute of Metals, London, 1990.
[31] K. Zazakowny, J. Lewandowska-Łańcucka, J. Mastalska-Popławska, K. Kamiński, A. Kusior, M. Radecka, M. Nowakowska, Biopolymeric hydrogels—nanostructured TiO_2 hybrid materials as potential injectable scaffolds for bone regeneration, Colloids Surf. B: Biointerfaces 148 (2016) 607–614.
[32] J. Li, X. Wang, R. Hu, H. Kou, Structure, composition and morphology of bioactive titanate layer on porous titanium surfaces, Appl. Surf. Sci. 308 (2014) 1–9.
[33] T. Mano, Y. Ueyama, K. Ishikawa, T. Matsumura, K. Suzuki, Initial tissue response to a titanium implant coated with apatite at room temperature using a blast coating method, Biomaterials 23 (2002) 1931–1936.
[34] A. Valanezhad, K. Tsuru, M. Maruta, G. Kawachi, S. Matsuya, K. Ishikawa, Zinc phosphate coating on 316L-type stainless steel using hydrothermal treatment, Surf. Coat. Technol. 205 (2010).